Band Structure of Periodically Surface-Scattered Water Waves

By TOM CHOU

Dept. of Applied Maths. & Theoretical Physics, University of Cambridge, Cambridge CB3 9EW

(Received March 7, 1997 and in revised form ??)

We employ Bloch wavefunctions similar to those used in calculating electronic and optical band gaps in solid state physics to derive dispersion relations for water wave propagation in the presence of an infinite array of periodically arranged surface scatterers. For one dimensional periodicity (stripes), band gaps for wavevectors in the direction of periodicity are found corresponding to certain frequency ranges which support only nonpropagating standing waves as a consequence of multiple Bragg scattering. The dependence of these band gaps as a function of scatterer density, strength, and water depth is analyzed. We find that in contrast to band gap behavior in electronic, photonic, and acoustic systems, these gaps can *increase* with excitation frequency ω. Thus, higher order Bragg scattering can play a dominant role in suppressing wave propagation. Furthermore, in one dimension, an additional constraint (in addition to single scatterer energy and momentum conservation) on the calculation of transmission T and reflection R coefficients of a *finite* number of scatterers is calculated from the exact dispersion relation of the infinite *periodic* system. This relationship may be useful in measurements where only phase or amplitude is easily measured. In simple two dimensional periodic geometries, we find no complete band gaps, implying that there are always certain directions which support propagating waves; we offer semi-quantitative reasons for why this is so. The role of evanescent modes is discussed, and finally, equations for water wave band structure in the presence of a uniform flow are derived.

1. Introduction

Wave diffraction is ubiquitous in Nature and important for countless technological applications. One application is sea surface wave interactions with natural and man-made structures. Coastlines as well as off-shore structures are susceptible to wave forces, and much research has focused on diminishing these interactions with the aim of designing more effective off-shore rigs, breakwaters, and docks (see for example Mei, Hara & Naciri (1988), Mei (1983) and Porter & Evans (1995)). Wave interactions with ice in polar waters is another important aspect of surface wave scattering. Different ice floe structures and distributions modify the sea surface wave spectra and must be considered when analyzing remote and direct wave sensing data and models of wind wave generation and oceanic transport (Wadhams et al. (1986)).

The theories behind wave diffraction have a rich history of development in many areas of physical science. In most scattering problems, for example those involving acoustic, electromagnetic, or electronic wave functions, the governing equation is a second order linear wave equation of the Helmholtz type. Usually, two boundary conditions are satis-

fied at the interface of scattering bodies, along with a radiation condition far away from the body. These prescriptions uniquely solve most scattering problems.

However, although surface perturbations on an ideal fluid propagate as waves, and general principles of scattering theory from other contexts apply, the equation governing the fluid velocity in the bulk liquid has no spatial variation. Thus, scattering can occur only through interactions with localized geometrical variation of the boundaries, or localized variations in the conditions imposed at the boundaries. An example of the former is the scattering of water waves from variations in bottom depth studied by Mei (1985), Belzons, Guazzelli & Parodi (1988), Davies, Guazzelli & Belzons (1989) and Mitra & Greenberg (1984). This problem has many important applications, including underwater breakwaters (Mei, Hara & Naciri (1988)), long distance ocean wave propagation (Elter & Molyneaux (1972)), wave propagation over rippled beds near beaches (Mei (1985), Naciri & Mei (1988), Davies, Guazzelli & Belzons (1989) and Kirby (1986)), and third sound propagation of superfluid helium films as discussed by Kleinert (1990). Characterizing surface waves can also be a means of remote sensing of bottom topographies. For abrupt jumps in bottom depth geometry, eigenfunction expansions of velocity and pressure are usually matched at these regions. The infinite number of poles in surface water wave dispersion is an indication that near scatterers, an infinite number of evanescent modes are required to match boundary conditions (see Eqn (A1)). Periodic bottom depths, or periodically arranged impenetrable obstacles piercing the sea surface, have also been studied theoretically with multiple scattering analyses by Mei (1983), Porter & Evans (1995), Kagemoto & Yue (1986). Integral equation techniques have been applied to study periodic breakwaters (Fernyhough & Evans (1995)) and bottom depths (Black, Mei & Bray (1971)). In these studies the possibility of resonant Bragg scattering from finite structural arrays was recognized by Mei (1983), Davies, Guazzelli & Belzons (1989), Mitra & Greenberg (1984); however, only first order Bragg scattering has been discussed. The problem of random bottoms can also be studied, especially using shallow water theory, where interesting localization behavior has been theoretically predicted and experimentally observed by Devillard, Dunlop & Souillard (1988), and Belzons, Guazzelli & Parodi (1988) and Elter & Molyneaux (1972), respectively.

In this paper we consider scattering that occurs when the parameters in the boundary conditions are spatially varying along the interface. Physical examples can be found on widely varying scales where surface tension or surface bending rigidity modulate periodically. For example, Lucassen-Reynders & Lucassen (1969) show that surfactant deposition at the air-water interface drastically attenuates wave propagation, and multiple surface wave scattering from surfactant concentration variations is thought to be one contributing mechanism as suggested by Chou and Nelson (1994). Moreover, monolayers of surfactants at air-water interfaces can phase separate into periodic domains as a consequence of line tension and microscopic dipolar interactions (Andelman, Brochard & Joanny (1987) and Knober & Desai (1992)). Similarly, ice floes, which vary the surface mass density as well as contribute bending moments to the air-sea interface, also scatter water waves and attenuate wave energy in Marginal Ice Zones (MIZ) (Fox & Squire (1990) and Squire et al. (1995)). Here, regular patterns of surface ice thickness can form due to periodic convection of freezing surface waters, or current instabilities of a freezing mushy ice zone. Also, stress from incident water waves on an ice sheet can break strips of ice off the leading edge and form very long, regular stripes of ice separated by open sea (Squire et al. (1995)). An approximate two-dimensional periodicity also exists in regions of pancake ice, where circular floes occupy

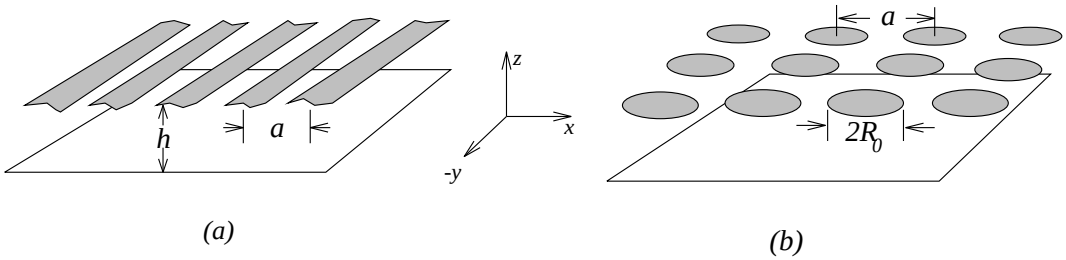

FIGURE 1. Schematic of periodic scatterers at the liquid interface. The depth is a constant h, and the bending rigidity and/or surface tension is D_2 and/or σ_2 inside the hatched regions and D_1 and/or σ_1 outside. Depicted here are scatterers which have sharp discontinuities in D and σ along the surface, in (a) one-dimensional stripes and (b) square array of disks of radius R_0.

a high filling fraction of the surface. All of the physical systems mentioned are schematically depicted in Figure 1 in the limit of perfect periodicity.

The connection to the classic problem of single obstacle scattering studied for example by Greene & Heins (1953) and Ursell (1957) is worth mentioning. The limit of thin surface obstacles, the prototypical problem of a semi-infinite or finite dock, has been studied extensively using various sophisticated applied mathematical methods such as integral equations (Friedrichs & Lewy (1948)) and Wiener-Hopf techniques (Greene & Heins (1953), Heins (1956)). In these problems, the fluid normal velocity at a simple surface region (half-space or strip) is constrained to vanish. Surface bending moments however, have been shown to be important for the study of water wave propagation in flexible docks and ice by Liu & Mollo-Christensen (1988). Reflection and transmission coefficients of water wave scattering from a semi-infinite flexible dock have been calculated using variational methods and numerical solution of integral equations by Squire et al. (1995) and Meylan & Squire (1994); however, only the amplitudes have been explicitly calculated. When considering multiple scattering, however, the phase is a critical variable to be considered as it affects whether waves interfere constructively or destructively. Wiener-Hopf techniques applied directly to the differential equations (Noble (1958), Heins (1956)) of motion are inapplicable when a semi-infinite dock has surface tension or bending rigidity since the proper solution requires a higher order discontinuity at the boundary between free water and the dock edge to conserve vertical stresses or bending moments, and ultimately energy (this failure is apparent when one considers the discontinuity in surface tension $\sigma(x)$ giving a $\delta(x)$ in Eqn. (2.8)). The more rigorous integral formulation of the Wiener-Hopf method by Krein (1962) may prove useful in solving the semi-infinite, flexible dock problem. An integral equation solution to the reflection and transmission coefficients of scattering from a semi-infinite surface tension discontinuity has been found by Gou, Messiter & Schulze (1993), but the energy conservation was applied *a posteori* and phase shifts were not found. Meylan & Squire 1994 have calculated the diffracted wave field from a circular sheet of flexible ice by matching many evanescent modes in a Green's function expansion. The circular surface tension contrast problem has also been treated by Chou, Lucas & Stone (1995) using dual integral equations.

Despite the technical difficulties in calculating scattering from single scatterers, we will show that an exact solution to an infinite *periodic* array of surface scatterers (such as ice floes) can be simply calculated. The results represent the effects of multiple scattering and allow easy physical interpretation. When used with certain robust wave properties such as energy and momentum conservation, and radiation conditions, the solutions can

yield useful relationships in the *single* surface scatterer problem. Numerous other physical results, interpretations, and implications for applications can also be gleaned.

In the following Section we formulate the model describing surface wave propagation in the presence of an infinite periodic array of surface deformable scatterers (Fig. 1). We adapt standard techniques used in solid state physics to describe periodic electronic wave functions to study surface water waves. Other applications of periodic scattering arise in the study of acoustic and photonic band gaps in periodic inclusions and colloidal crystals, respectively. In our problem, the surface boundary conditions supply the periodicity and are cast into matrix equations with the dispersion relation of an infinitely periodic system determined by the spectrum of eigenvalues.

In the Results and Discussion, Section 3, we consider both one and two-dimensional arrays of surface scatterers; wave propagation of course, can occur in any direction in the (x, y)-plane (see Fig 1). The physical features of the dispersion relations are displayed and qualitatively explained. We find band gaps, (also often denoted as stop gaps) analogous to those found in other systems (Ashcroft & Mermin (1976), McCall et al. (1991), Sigalas & Economu (1992)), where as a consequence of the coupling between the periodic nature of the scatterers and the plane waves, the dispersion curves $\omega(q)$ have jumps between which the excitation frequencies do not correspond to extended plane waves, but rather localized states corresponding to complex wave vectors. The location of these jumps in ω as a function of wavevector $\vec{q}$ define Bragg points (1D) or lines (2D) in Fourier space where resonant multiple scattering occurs (Ashcroft & Mermin (1976) and Joanopoulos, Meade & Winn (1995)), and large distance propagating modes cancel. For one-dimensional periodicities, an approximate form is given for the splitting of doubly degenerate eigenvalues into a gap. We emphasize the physical phenomena of band gaps and their dependences on parameters such as scattering strength and water depth, we will not provide an exhaustive array of numerical calculations. We also briefly discuss the differences between water wave scattering and wave scattering derived from a "local" Helmholtz equation. In particular the effects of the decaying "evanescent" components near the scatterers are discussed.

In the Summary and Conclusions, we briefly mention the general features of the basic results and their implications for multiple scattering in natural and manmade applications, such as wave propagation in ice fields and arrays of surface plates. In the Appendices, we use a remarkably simple but general analysis of one dimensional symmetric scatterers, to derive in certain limits, the band gaps as a function of transmission/reflection coefficients and their phases. Therefore, upon comparison with the exact results of Section 3, we obtain an additional constraint on transmission and reflection coefficients (including their phases) of a finite number n one-dimensional symmetric surface scatterers of arbitrary strength. We also outline the equations required to treat periodically surface scattered water wave propagation in the presence of underlying uniform flows.

2. Model of Periodic Surface Waves

In this section, we formulate the the dynamics of an interface overlying an ideal fluid of depth h (Fig. 1). Balance of surface stresses leads to dynamical equations which govern surface wave propagation. We restrict our analysis to *surface* scatterers. These structures are assumed to have small thicknesses d ($d \ll \lambda, h$, where λ is any wavelength) and lie entirely at the water interface $z \simeq 0$ and thus do not change the domain over which Laplace's equation for the velocity potential holds. Examples are thin plates with bending stiffness or domains of surface active materials which locally decrease surface

tension. The scatterers are periodic and their in-plane interfacial positions are assumed fixed.

2.1. *Surface Water Waves*

The motion of the interface is coupled to the bulk flow which is described by the linearized Navier-stokes equation for incompressible ideal flows,

$$\partial_t \mathbf{v} + (\mathbf{v}\cdot\nabla)\mathbf{v} = -\frac{1}{\rho}\nabla p + \rho\vec{g}. \qquad z < \eta(\vec{r},t) \tag{2.1}$$

where ρ is the bulk fluid density, $\rho\vec{g} \equiv -\rho g\hat{z}$ is the external body force density due to gravity, p is the pressure, and $\eta(\vec{r},t)$ is the surface deformation as a function of surface coordinate $\vec{r} \equiv (x,y)$. We neglect all dynamical effects of the upper fluid, air. By assuming irrotational flows, the velocity can be expressed in terms of a potential, $\mathbf{v} \equiv \nabla\varphi$. Hence,

$$\nabla\cdot\mathbf{v} = \nabla^2\varphi(\vec{r},z,t) = (\nabla_\perp^2 + \partial_z^2)\varphi(\vec{r},z,t) = 0. \qquad z < \eta(\vec{r}) \tag{2.2}$$

where $\nabla_\perp^2 \equiv \partial_x^2 + \partial_y^2$ is the 2D Laplacian in the coordinates of Fig. 1. The linearized kinematic conditions at the free interface and the bottom $z = -h$ are

$$\lim_{z\to 0^-} \partial_z\varphi(\vec{r},z,t) = \partial_t\eta \tag{2.3}$$

and

$$\lim_{z\to -h^+} \partial_z\varphi(\vec{r},z,t) = 0. \tag{2.4}$$

The linearized normal fluid stress at the interface is,

$$P_{nn} \equiv \lim_{z\to 0^-} \rho\left[\partial_t\varphi + g\eta(\vec{r},t)\right] \simeq P_{zz}, \tag{2.5}$$

where we have assumed the absence of externally imposed stream flow and that the only disturbances are in the form of dynamic surface waves. The fluid stress P_{nn} is balanced by spatially periodic varying material restoring forces from the surface scatterers, such as those due to surface bending and stretching. In the absence of fluid viscous stresses, the application of surface stresses must be carefully applied to ensure conservation of $z-$ component forces, torques, and bending moments. These forces and the energy are manifestly conserved when the surface stresses are derived from an energy functional for the bulk fluid plus interface. For example P_{zz} and gradients of $\sigma(\vec{r})$ have to be considered in inviscid fluids to conserve wave energy. Thus, the net $\hat{z}$-component surface stress balance reads

$$\left[\nabla_\perp\cdot(\sigma(\vec{r})\nabla_\perp) - \nabla_\perp^2(D(\vec{r})\nabla_\perp^2)\right]\eta(\vec{r},t) = P_{zz} \tag{2.6}$$

which upon taking the time derivative and using (2.3) yields

$$\lim_{z\to 0^-}\left[\nabla_\perp\cdot(\sigma(\vec{r})\nabla_\perp) - \nabla_\perp^2(D(\vec{r})\nabla_\perp^2)\right]\partial_z\varphi(\vec{r},z,t) = \partial_t P_{zz}, \tag{2.7}$$

where $D(\vec{r})$ and $\sigma(\vec{r})$ are the flexural rigidity and surface tension respectively. In Eqn. (2.7), we have neglected the rotational inertial terms in the surface bending stresses. Recall that in thin plate theory, $D = Ed^3/12(1-s^2)$ where E and s are Young's modulus and Poisson's ratio of the surface material in its *bulk* phase. For open water between

the thin plates, $D_1 = 0$. A physical example is a large sheet of sea ice with alternating thickness.

We will only consider, for all dynamical variables, time variations of the form $e^{-i\omega t}$. The neglect of rotational inertia terms is thus valid when $\omega^2 \ll E\rho_i^{-1}\lambda^{-2}$, which holds for most applications. In the frequency domain, we combine the time derivative of the $z-$component stresses and use (2.3) to obtain

$$\lim_{z\to 0^-}\left[\rho\omega^2\varphi(\vec{r},t) - \left(\rho g - \nabla_\perp\cdot(\sigma(\vec{r})\nabla_\perp) + \nabla_\perp^2\left(D(\vec{r})\nabla_\perp^2\right)\right)\partial_z\varphi(\vec{r},z,t)\right] = 0 \tag{2.8}$$

Equation (2.8) and (2.2) determine the velocity potential which has a $e^{-i\omega t}$ time dependence. The effects of spatially varying surface properties are implicit in the boundary condition (2.8). In the limit of *uniform* $\sigma(\vec{r}) = \sigma$ and $D(\vec{r},t) = D$, $\varphi \propto e^{\pm i\vec{k}\cdot\vec{r}}\cosh k(h+z)$, from which we obtain the standard dispersion relation

$$\omega^2 = \left(gk + \frac{\sigma}{\rho}k^3 + \frac{D}{\rho}k^5\right)\tanh kh. \tag{2.9}$$

This expression is valid far from (at least many wavelengths from) spatial inhomogeneities of the surface parameters $\sigma(\vec{r})$ and $D(\vec{r})$.

However, when σ and/or D are not uniform, surface waves diffract/refract from the regions of varying surface properties and the Fourier modes of the velocity potential at the interface mix with those of the surface variations. The rest of this paper deals with periodic variations in $\sigma(\vec{r})$ and $D(\vec{r})$ where the boundary condition (2.8) is to be used to solve $\nabla^2\varphi$.

2.2. *Bloch Functions and Periodic Solutions*

The following analysis is similar to the treatment of a single particle electronic wave function in a periodic potential. Details are given in Ashcroft & Mermin (1976). Another application can be found in photonic crystals where light propagation through a medium with periodic inclusions of different dielectric constants is studied, Joanopoulos, Meade, & Winn, (1995). These references describe in detail the terminology used; however, our problem contain some minor differences and we give a largely complete formulation below.

Near sources or variations in σ or D, the velocity potential must be decomposed into a complete set of eigenfunctions. The choice

$$\varphi(\vec{r},z) = \sum_{\vec{q}}\varphi_{\vec{q}}\,e^{i\vec{q}\cdot\vec{r}}\,\frac{\cosh q(h+z)}{\cosh qh}, \tag{2.10}$$

with $q \equiv \lim_{\epsilon\to 0}\sqrt{q^2+\epsilon^2}$ manifestly satisfies Laplace's equation and (2.4). For the surface scatterers we consider one and two-dimensional periodicities, with lattice vectors $\vec{a}$ (see Fig. 1). Since the surface properties are periodic in $\vec{a}$, (*i.e,* $D(\vec{r}+\vec{a}) = D(\vec{r})$) they can be Fourier decomposed according to

$$\sigma(\vec{r}) = \sum_{\vec{G}}\sigma(\vec{G})e^{i\vec{G}\cdot\vec{r}} \tag{2.11}$$

$$D(\vec{r}) = \sum_{\vec{G}}D(\vec{G})e^{i\vec{G}\cdot\vec{r}} \tag{2.12}$$

where $\vec{G}$ are the corresponding reciprocal lattice vectors. The reciprocal lattice vectors for stripe, square, and triangular lattices with periodicity a are

$$\begin{aligned}
\vec{G} &= \frac{2\pi m}{a}\hat{x} \equiv m\vec{G}_0 && \text{(stripes)} \\
\vec{G} &= \frac{2\pi m}{a}\hat{x} + \frac{2\pi n}{a}\hat{y} && \text{(square)} \\
\vec{G} &= \frac{4\pi m}{\sqrt{3}a}\hat{x} + \frac{2\pi n}{\sqrt{3}a}(\hat{x} - \sqrt{3}\hat{y}) && \text{(triangular)}
\end{aligned} \tag{2.13}$$

with m, n integers. Any particular reciprocal lattice vector in the set $\{\vec{G}\}$ for each type of lattice can be constructed by a countable number of others. We now exploit the periodicity of $D(\vec{r})$ in the boundary condition (2.8) and use Bloch's theorem which states that a function with periodic interactions and boundary conditions can be written in terms of a phase factor times a function invariant under discrete translations of the periodicity, $\varphi(\vec{r}, z) \equiv e^{i\vec{q}\cdot\vec{r}}\phi(\vec{r})$. The function $\phi(\vec{r}+n\vec{a}) = \phi(\vec{r})$ can be Fourier represented in a manner identical to $D(\vec{r})$ or $\sigma(\vec{r})$. Bloch's theorem and periodic boundary conditions on the entire array of scatterers (Born-von Karman boundary conditions) require $\vec{q}$ to be real and have the form (Ashcroft & Mermin (1976))

$$\vec{q} = \frac{n_i}{N_i}\vec{G}_0(i) \tag{2.14}$$

where N_i is the large number of scatterers in the i^{th} lattice direction, and $\vec{G}_0(i)$ is the unit reciprocal lattice vector in the i^{th} direction. The granularity of $\vec{q}$ is thus determined by the total number of scatterers that we apply the periodic boundary conditions to. Direct substitution of either $e^{i\vec{q}\cdot\vec{r}}\phi(\vec{r})$ or (2.10) and (2.12) into (2.8) yields for each independent Fourier component

$$\begin{aligned}
\rho\left(\omega^2 - \Omega^2_{\vec{q}}(\vec{G})\right)\varphi_{\vec{q}}(\vec{G}) = \sum_{\vec{G}'\neq\vec{G}} \Big[&|\vec{q}-\vec{G}|^2|\vec{q}-\vec{G}'|^3 D(\vec{G}-\vec{G}') + \\
&(\vec{q}-\vec{G}')\cdot(\vec{q}-\vec{G})|\vec{q}-\vec{G}'|\sigma(\vec{G}-\vec{G}')\Big] \tanh|\vec{q}-\vec{G}'|h\,\varphi_{\vec{q}}(\vec{G}')
\end{aligned} \tag{2.15}$$

where

$$\Omega^2_{\vec{q}}(\vec{G}) \equiv \left(g|\vec{q}-\vec{G}| + \frac{\sigma_0}{\rho}|\vec{q}-\vec{G}|^3 + \frac{D_0}{\rho}|\vec{q}-\vec{G}|^5\right)\tanh|\vec{q}-\vec{G}|h \tag{2.16}$$

and $\sigma_0 = \sigma(\vec{0})$ and $D_0 = D(\vec{0})$ are the spatially averaged surface properties. Equation (2.16) is the fundamental matrix equation that determines the relationship between frequency ω and wavevector $\vec{q}$. For the sake of mathematical clarity and simplicity, we will consider the case where $\sigma = 0$ relevant for long gravity waves ($\lambda \geq 2$cm), or short bending waves ($\lambda \leq 2\pi(g/D)^{1/4}$). Thus the scattering originates only from the the periodically varying bending rigidities at the interface. The extension to include $\sigma(\vec{G}) \neq 0$ for studying surface waves in the presence of periodic surfactant coverage is straightforward. Note that in Eqn. (2.16), $\varphi_{\vec{q}}(\vec{G})$ is invariant to shifts in $\vec{G}$. In other words there is only a set of $\prod_i N_i$ $\vec{q}$'s that uniquely determines $\varphi_{\vec{q}}$. Thus, the $\Pi_i N_i$ coefficients are coupled ($\varphi_{\vec{q}}(\vec{0})$, $\varphi_{\vec{q}}(\vec{G})$, $\varphi_{\vec{q}}(\vec{G}')$, etc.) by as many equations. We have therefore shifted the wavevector by $\vec{G}$ such that $\vec{q}-\vec{G}$ falls within the boundaries delineated by the first

Bragg planes, *i.e.* the first Brillouin zone. Only the $\prod_i N_i$ number of $\vec{q}$'s need be considered, and we will eventually represent this by plotting in the reduced zone scheme, where $\vec{q}$ only takes on values in that part of the first Brillouin zone irreducible by symmetry. For example, in one dimension, the Bragg planes are points at $q_x = \pm\pi$; however, we need only plot $\omega(q_x)$ in the region $0 \leq q_x < \pi$.

Note that we are considering a linearly stable nondissipative system and all eigenvalues $\rho\omega^2$ are real. The matrix (2.16) can be written in an inherently symmetric form by considering normalized Fourier coefficients $\varphi'_{\vec{q}}(\vec{G}) = |\vec{q}-\vec{G}|\tanh|\vec{q}-\vec{G}|h\,\varphi_{\vec{q}}(\vec{G})$. The problem is therefore a generalized eigenvalue problem $\mathbf{A}'\varphi'_{\vec{q}} = \rho\omega^2\mathbf{B}\varphi'_{\vec{q}}$ where $\mathbf{B}$ is diagonal. Applying the inverse of the square root of $\mathbf{B}$ to both sides (Cholesky decomposition), the problem is recast into a symmetric eigenvalue problem,

$$\det|\mathbf{A} - \rho(\omega^2 - \Omega_{\vec{q}}^2)\mathbf{1}| = 0, \tag{2.17}$$

where

$$\mathbf{A}(\vec{G}\neq\vec{G}') = D(\vec{G}-\vec{G}')|\vec{q}-\vec{G}|^{5/2}|\vec{q}-\vec{G}'|^{5/2}\tanh^{1/2}|\vec{q}-\vec{G}|h\tanh^{1/2}|\vec{q}-\vec{G}'|h. \tag{2.18}$$

The above symmetrization facilitates the calculation and computational convergence of the eigenvalues $\rho\omega^2$.

We now consider example one and two-dimensional periodic "surface potentials" $D(\vec{G}-\vec{G}')$. In one dimension, we consider square notch scatterers corresponding to a surface sheet with alternating bending rigidities $D(x) = D_1$ or $D(x) = D_2$ depending on whether x is inside or outside a strip, respectively (see Fig 1(a)). For two-dimensional periodic surface scatterers, we consider both square (Fig 1(b)) and triangular (not shown) lattices of circular disks of radius R_0. Inside each disk, $D = D_2$, while outside $D = D_1$. The Fourier transforms in reciprocal lattice vector space for the above scattering potentials are, $D(\vec{0}) \equiv \bar{D} = (1-f)D_1 + fD_2$, and

$$\begin{aligned} D(\vec{G}\neq\vec{0}) &= \frac{D_2-D_1}{\pi|\vec{G}|}\sin(|\vec{G}|af) \qquad \text{1D periodicity} \\ D(\vec{G}\neq\vec{0}) &= 2f\frac{(D_2-D_1)}{|\vec{G}|R_0}J_1(|\vec{G}|R_0) \quad \text{2D periodicity,} \end{aligned} \tag{2.19}$$

where f is the fraction of area covered by the D_2 material, and $\vec{G}$ is the appropriate reciprocal lattice vector for the surface periodicity under consideration. Our choices above are numerically the most laborious due to Gibb's phenomenon at the sharp discontinuities in $D(\vec{r})$; nonetheless, we find the eigensolutions to (2.18) converge rapidly as a function of matrix size.

As a consequence of a periodic differential operator, $\nabla_\perp^2(D(\vec{r})\nabla_\perp^2)$, the band gaps in the water wave dispersion relation will, unlike periodic scattering in electronic, optical, and acoustic systems, more likely increase initially as frequency increases. This prediction is apparent when we consider relatively weak scatterers D such that $\frac{1}{2}|\vec{G}|\bar{D} \gg D(|\vec{G}|)$ where for certain $\vec{G}$ we can obtain an approximate analytic approximation for the band gaps in ω^2. Using degenerate perturbation theory at $\vec{q}-\vec{G}$ near Bragg planes is tantamount to truncating $\mathbf{A}$ into block $m\times m$ matrices for m frequencies that are closely spaced. For simplicity, we consider one dimensional square stripes where doubly degenerate frequencies near the n^{th} Bragg planes ($q_x = 0, \pi$) are split according to

$$\omega_{\pm}^2 \simeq \left[g + \frac{\bar{D}}{\rho} \left(\frac{n\pi}{a}\right)^4 \pm \left(\frac{n\pi}{a}\right)^4 \frac{(D_2 - D_1)}{\rho n\pi} \sin(n\pi f) \right] \left(\frac{n\pi}{a}\right) \tanh\left(\frac{n\pi}{a} h\right) \qquad (2.20)$$

The stop band splittings increase with order as $(D_2 - D_1)n^4 \sin(n\pi f)$, although the absolute frequencies where they are found also increase as $\bar{D}n^5$ in this weakly scattered limit. Similar expressions can be found for the band gaps near Bragg planes in two-dimensionally periodic systems.

3. Results and Discussion

We numerically solve the eigenvalue problem represented by Eqns. (2.17) and (2.18) using standard methods (Press *et al.*, 1992). Typically, 256 plane waves (different $vecG$'s) are taken for both the one and two-dimensional cases, such that the lowest 4-6 eigenvalues do not change appreciably ($< 1\%$) upon doubling the matrix size. The calculations converge very efficiently for the lowest 4-6 eigenvalues especially in two dimensions because the extra Bessel function J_1 make the off-diagonal elements fall off faster. The matrix calculations for smoother variations in $D(\vec{r})$ become extremely simple; for example, $\mathbf{A}$ is tridiagonal when D is sinusoidal.

Analysis of the following results will give a consistent qualitative picture of multiple scattering effects and surface wave propagation in the presence of periodic bendable plates. In our numerical plots, all distances are scaled with respect to lattice spacing, and wavevectors are measured in units of a^{-1}. The frequency is nondimensionalized and measured in units of $\sqrt{g/a}$, and the bending rigidity is measured in units of $\rho g a^4/\pi^4$.

3.1. *One Dimensional Periodicity*

The choice $D_1 = 0$, $D_2 \neq 0$ is appropriate for open water punctuated by flexible strips and illustrates the difference between gravity and bending waves. For concreteness, in the scattering strips, we choose $D_2 = 3.0$, which for the Young's modulus and Poisson's ratio of sea ice ($E = 6 \times 10^{10}$dynes/cm and $s = 0.3$), and periodicities of 1.0m, corresponds to a $d \sim 0.8$cm cover of ice. At this coverage, the dispersion within the ice sheet is predominately determined by bending forces (compare the terms gq and $D_1 q^5/(\rho a^4)$) except at large wavelengths ($q \leq \pi/2$).

The first few bands in the dispersion relation for wave propagating in an array of one-dimensional periodic surface scatterers are plotted in Figure 2. Here, the depth $h = \infty$, the filling fraction $f = 0.6$, and $D_2 = 3.0$. The right panel shows the dispersion relation for $q_y = 0$ as a function of q_x, the wavevector in the direction of periodicity. We have plotted the axis according to the reduced zone scheme were the dispersion relations are folded at every half unit reciprocal lattice vector $\vec{G}_0$, *i.e.* every Bragg plane. The band indices n correspond to the number of half reciprocal lattice base vectors $\vec{G}_0/2 = \hat{x}\pi/a$ included in the $\hat{x}$-direction wavevector (the notation for q_x and the n^{th} order band gaps is shown in Fig. 3). Note the wider higher order gaps in Fig. 2. These gaps are simply discontinuities in the spectrum as wavevector parameter is increased and are associated with Bragg scattering planes. Physically, they are standing waves where the lower frequency branch corresponds to oscillations with most of the wave nodes(antinodes) located in the low(high) $D(\vec{r})$ regions, D_1 and D_2 here respectively. The higher frequencies are clearly associated with a translation of these low frequency standing waves, and have more nodes in the D_2 regions. The left panel shows ω as a function of q_y. However, in the reduced zone scheme, only the lowest branch ($n = 0$) corresponds to a wave propagating solely in the $\hat{y}$ direction. Interestingly, the motions

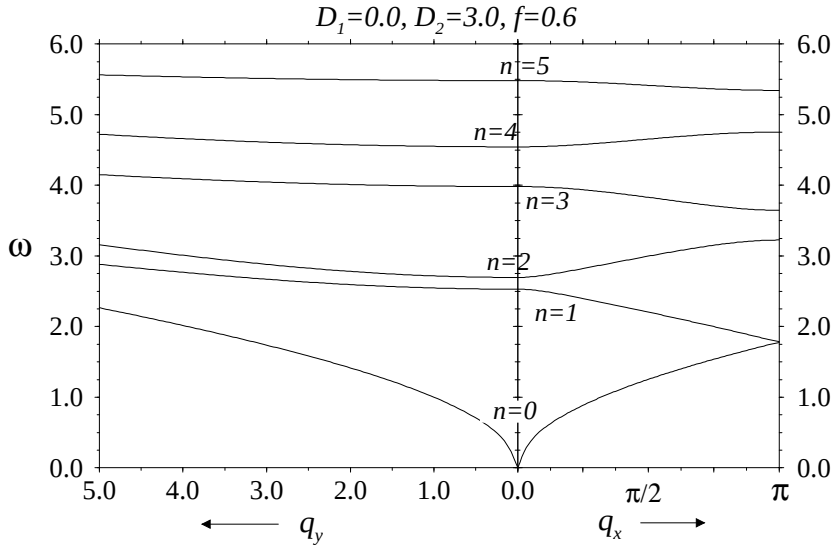

FIGURE 2. The dispersion relation, or band structure of surface waves (with $h = \infty$) in the presence of stripes of discontinuous $D(x)$. Lengths are measured in units of periodicity a and frequencies are measured in units of $\sqrt{g/a}$. Surface values used are $\sigma = 0$, $D_1 = 0$, $D_2 = 3.0$, and filling fraction $w/a \equiv f = 0.6$. The right panel plots $\omega(q_x, 0)$, the left, $\omega(0, q_y)$, where $\omega(\vec{q}) = \omega(-\vec{q})$. The eigenfrequencies are plotted in the reduced zone scheme, where different bands n correspond to wavevectors displaced by $n\vec{G}_0/2 = n\pi/a\hat{x}$. Note the first small band gap between $\omega_{n=0}(\pi, 0) \simeq 1.77$ and $\omega_1(\pi, 0) \simeq 1.79$

corresponding to this mode has no variation in the $\hat{x}$ direction. Note that this wave has a predominantly gravity wave-like dispersion. The entire set of surfaces can be constructed by folding the page along the $x = 0$ axis and bending the left panel upwards. The surfaces are then bounded by the plotted curves. As a consequence of inversion symmetry, here, as well as in the two dimensional lattices, the dispersion relations are symmetric with respect to $\vec{q} \to -\vec{q}$. There are an infinite series of gaps in the q_x direction, however, since the bands increase indefinitely in the q_y direction, for any real ω, propagating modes in some direction can be found and *complete* (*i.e,* in *all* directions) band gaps do not exist. Complete gaps *may* exist in higher dimensions however, as they do in periodic optical and acoustic systems.

Shown in more detail in Fig. 3 is the first band gap at $q_y = 0$. The frequency range between $\omega_0(\pi, 0)$ and $\omega_1(\pi, 0)$ (labeled for $D_1 = 0.03, D_2 = 3.0$ only) correspond to frequencies where modes cannot propagate in the q_x direction. This fact can be shown by explicitly constructing the standing wave velocity potential within the gap frequencies, but can be seen more directly by considering the mode group velocities $\vec{c}_g = \partial_{\vec{q}}\omega(\vec{q})$. Note that $c_{g,x} \to 0$ as a Bragg plane is approached due to the inherent symmetry of the problem. The sensitivity to $D_1 \neq 0$ is also apparent. Notice that for $D_1 > 0$, the dispersion relation develops an upward curvature indicative of increasing bending wave characteristics, especially in the bottom panel. This trend exists in $\omega_0(0, q_y)$ as well.

We now explore the parameter dependence of the band structure. Figures 4(a) and (b) show the positions and widths of the first three band gaps as a function of depth h for filling fractions of $f = 0.8$ and $f = 0.97$ respectively. In both plots $D_1 = 0$ and $D_2 = 3.0$. The effects of h become important only in shallow water when $|\vec{q} - \vec{G}|h \leq 1$ and

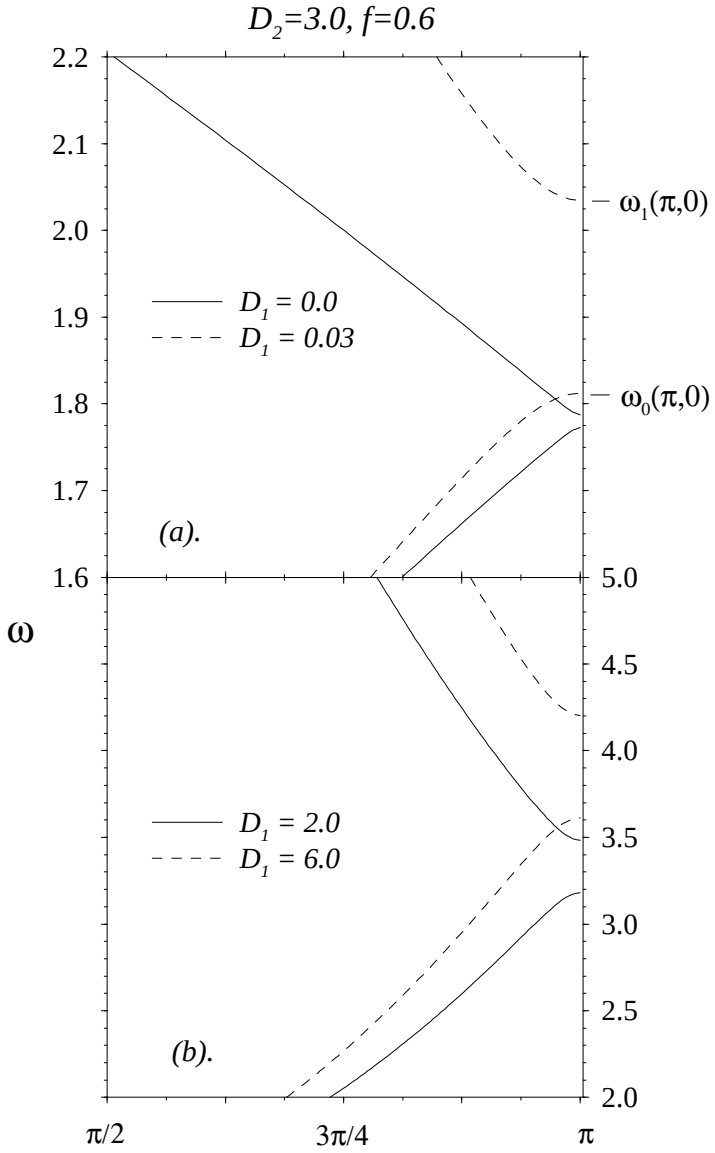

FIGURE 3. An expanded plot of the first band gap for various D_1. (a). Solid curves, $D_1 = 0.0$; dashed curves, $D_1 = 0.03$. The repeated zone notation is indicated. (b). Solid curves, $D_1 = 2.0$; dashed curves, $D_1 = 6.0$

manifests itself primarily through changing the excited wavelengths at fixed ω. Therefore, the higher order gaps (higher $|\vec{q} - \vec{G}|$) saturate to their $h \to \infty$ limit at smaller depths.

The gaps are most sensitive to the filling fraction f and D_1. Figure 5(a) shows the filling fraction dependence of the first three gaps for $D_1 = 0.0\,, D_2 = 3.0$, and $h = \infty$. The lower plot, Figure 5(b), shows the same three bands when $D_1 = 1.0$. Band gap widths are not monotonic functions of f and generally increase near larger values of f when $D_2 > D_1$. As expected, the gaps are spread to lower f as D_1 is increased and actually are larger for smaller f when $D_1 > D_2$ (not shown). All gaps disappear at $f = 0.0$

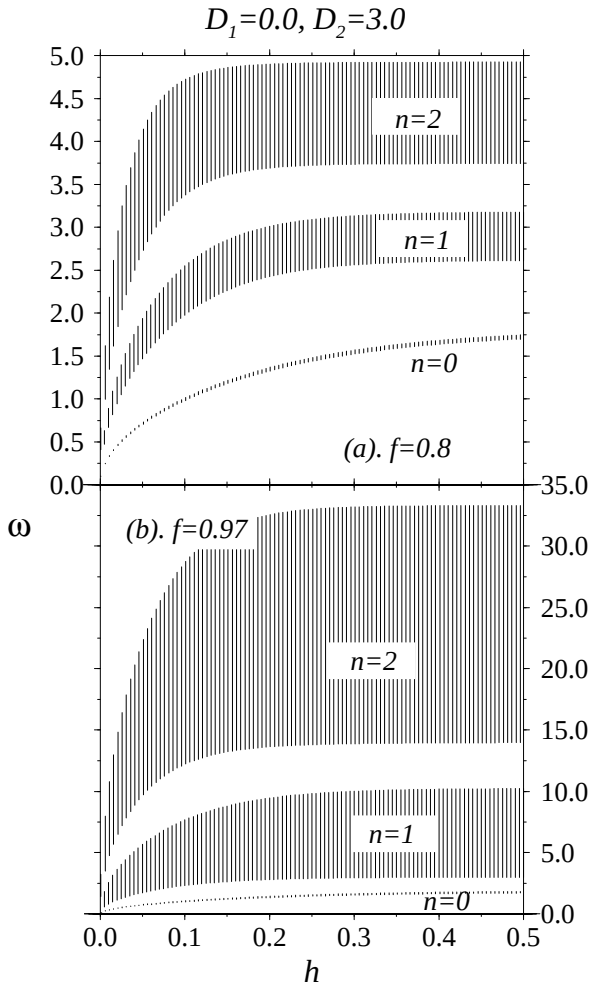

FIGURE 4. The first three band gaps as a function of water depth for $D_1 = 0.0\,, D_2 = 3.0\,, h = \infty$ at (a). $f = 0.8$ and (b). $f = 0.97$.

and $f = 1.0$ as the interface becomes uniform. Note that for the second (and higher) bands, the gap widths alternate and disappear for special values of f. This property is a consequence of the sinusoidal behavior of $D(\vec{G})$. Higher bands have qualitatively similar behavior but are at much higher frequencies, beyond the scales of Fig 5.

The variation in band gaps as a function of D_1 is also analyzed. The first, second, and third gaps as functions of D_1/D_2 ($D_2 = 3.0$) for $h = \infty$ and $f = 0.6$ and $f = 0.8$ are plotted in Figures 6(a), (b) and (c), respectively. The first gap, shown in Fig. 6(a) is most sensitive to variations in D_1 near $D_1 = 0$. The gap increases rapidly from a small constant value as D_1 is increased until it vanishes as D_1 approaches D_2, when the surface becomes uniform. At this point the dispersion relation is governed by Eqn. 2.9 in all directions. Figures 6(b), (c) however, show interesting reentrant behavior as D_1 is varied. There can be special values of $D_1 \neq D_2$ where the second and higher gaps vanish, similar to the vanishing of gaps as a function of f shown in Fig. 5.

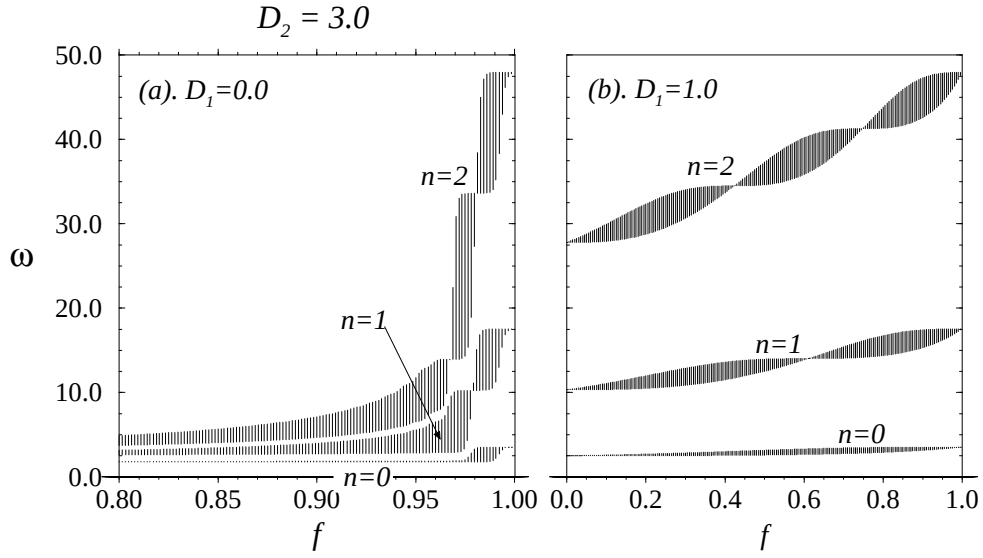

FIGURE 5. The first three band gaps, $\omega_1(\pi,0) - \omega_0(\pi,0)\,, \omega_1(0,0) - \omega_0(0,0)$, and $\omega_2(\pi,0) - \omega_1(\pi,0)$, as a function of filling fraction $f = w/a$ for (a). $D_1 = 0.0$ and (b). $D_1 = 1.0$, all other parameters are those of Fig 4.

3.2. *Two Dimensional Periodicity*

The two dimensional dispersion relations depend in a more complicated way on the direction of $\vec{q}$. We show the results for square and triangular lattices, where $|\vec{G}_0| = 2\pi/a$ and $R_0 = a\sqrt{f/\pi}$ for square lattices, and $|\vec{G}_0| = 4\pi/\sqrt{3}a$ and $R_0 = 3^{1/4}a\sqrt{f/2\pi}$ for triangular lattices. The first lowest bands for waves propagating in square and triangular lattices are plotted along the paths in the Brillouin zone depicted in the corresponding insets in Figure 7 (a) and (b) respectively. In the two-dimensional plots, we have chosen $D_2 = 100.0$ and $D_1 = 0.0$, corresponding to $d \sim 2.6$cm of ice when $a = 100$cm. We used $f = 0.3$ for the square lattice and $f = 0.4$ for the triangular lattice. Note that the maximum filling corresponding to close packing is $f = \pi/4$ and $\pi/2\sqrt{3}$ for the square and triangular lattices respectively. The dispersion relations shown in Fig. 7 may qualitatively represent monochromatic wave propagation through pancake ice zones. In Figure 7(a), the dashed curve corresponds to wave propagation over a uniform flexural rigidity of $\bar{D}$ in the repeated zone scheme. The qualitative features depicted in Fig. 7 are not as sensitive to the parameters as the one-dimensional periodicity considered above, although oscillations in the band gaps at Bragg points X and M also occur, though are less pronounced compared to $\omega(q_x)$ in the 1D model as f and D_1/D_2 are tuned.

3.3. *Complete Gaps, Boundaries, and Defects*

After a parameter search in f, $D_1\,, D_2$, and h, we find no complete low order band gaps in two dimensions: There are always certain directions in which waves can propagate. This property is in contrast to photonic and phononic band structure, where complete gaps have been found by Joanopoulos, Meade & Winn (1995), Kushwaha et al. (1993) and Sigalas & Economu (1992). The origins of this difference lie in nature of the wave scattering and the boundary conditions at the scatterer edges. Firstly, the dispersion caused by wave impedance mismatch due to variations in D is weak, *i.e,* since $\omega^2 \simeq$

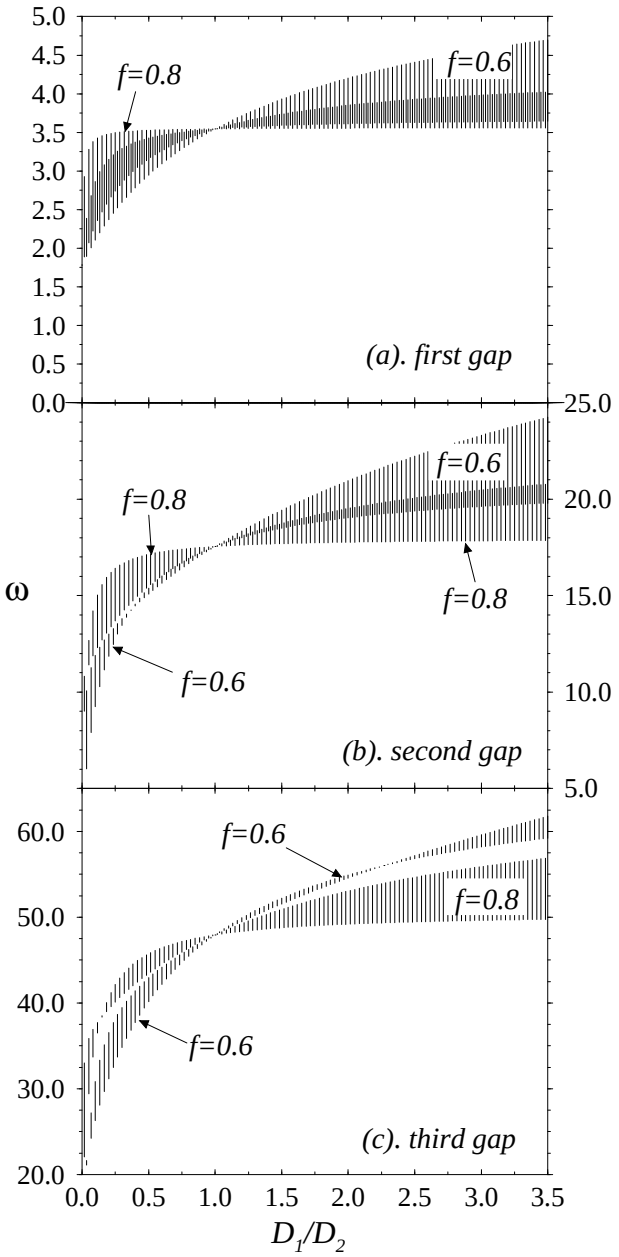

FIGURE 6. The first three band gaps, (a), (b), and (c), respectively as a function bending rigidity mismatch D_1/D_2 at infinite depth and filling fractions $f = 0.6$ and 0.8.

$D_i q^5$, D_i must change by a considerable amount for the wavelengths $2\pi/q$ that *would* be excited in an infinite domain of uniform D_i to change appreciably at any given ω. Secondly, although higher derivatives $\eta(\vec{r}, t)$ are required to be discontinuous, the lower derivatives are continuous which limits the reflection from an edge discontinuity in D. Thus, scattering is not particularly strong in this system. Furthermore, the evanescent modes can couple among the scatterers for high filling fractions. This is a direct analogy

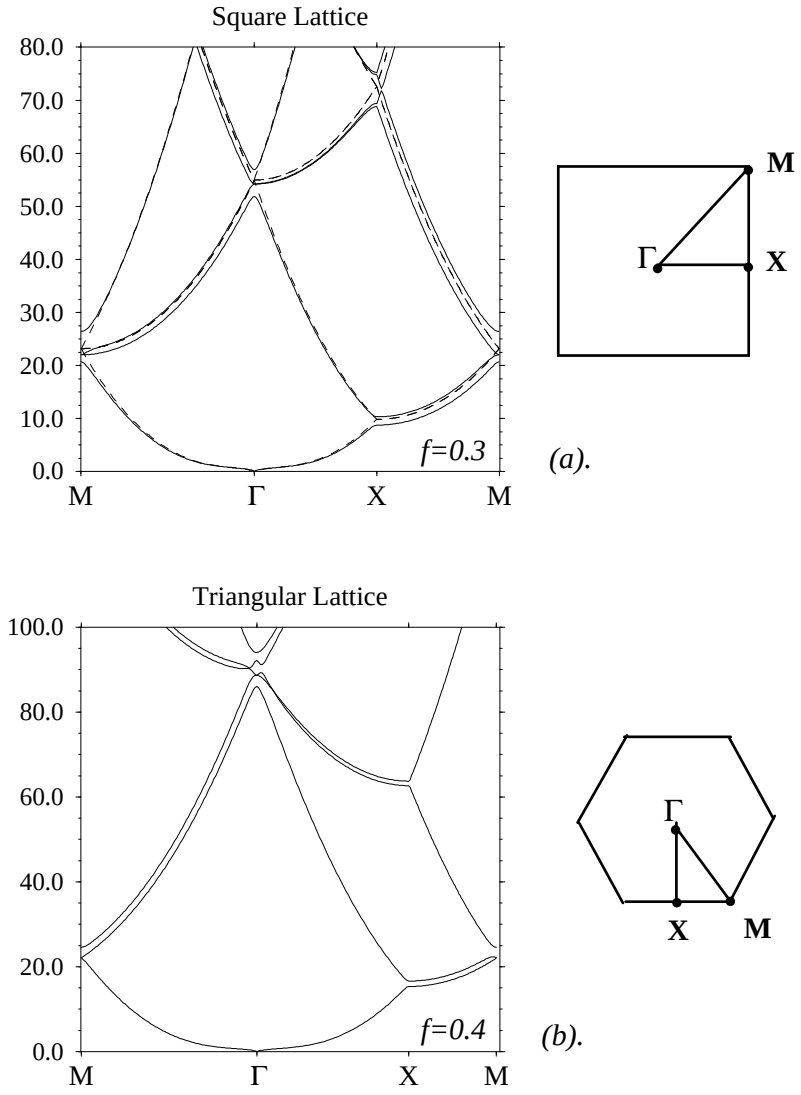

FIGURE 7. Two dimensional infinite depth band structure for (a). square and (b). triangular lattice of circular plates of radius R_0. $D_2 = 100.0\,, D_1 = 0$. The filling fractions f used are indicated.

to prism coupling of a totally internally reflected light ray at the edge of a prism. In the water scattering problem, these evanescent modes decay exponentially with a length scale set by the depth, (see Eqn. (A 3)) except in the $h \to \infty$ limit where they decay as a power law. Thus, evanescent modes in infinitely deep water can especially be potent in effectively coupling the surface scatterings and prevent wave localization and complete band gaps. Since the gap widths in any direction tend to increase at higher bands, one might expect that complete gaps can be found at higher frequencies (or energies); however, this is not likely either since the dispersion relations and the *positions* of the gaps are very sensitive to $q_x - \vec{G}$ at high frequencies, and the chances that gaps in all directions fall within each other are also diminished at high ω.

An interesting correspondence exists for gravity waves (uniform interface) in the presence of periodic bottom scatterers. The shallow water, depth averaged equation

$$\partial_t^2 \eta(\vec{r}) = g\nabla_\perp \cdot (h(\vec{r})\nabla_\perp)\eta(\vec{r}) \tag{3.1}$$

is isomorphic to the acoustic wave equations in a fluid (no shear modulus). However, although complete acoustic band gaps have been found in square lattice geometries (Sigalas & Economu (1992)), Eqn. (3.1) actually corresponds to *uniform* compressive moduli, but different material densities in the fluid acoustic scattering context. In other words, the speed of sound and the density difference are constrained such that $(c_1/c_2)^2 = \rho_2/\rho_1$ for the analogy with Eqn. (3.1) to hold. Under these conditions, Sigalas & Economu (1992) suggest there are no complete band gaps. Therefore, we conclude that the periodic bottom, shallow water wave problem has no complete band gap. A numerical search using the analogous matrix (2.16) for Eqn. (3.1) confirms the absence of a complete band gap.

We have only quantitatively treated an infinite (periodic boundary condition) perfectly periodic array of scatterers. However, in real physical situations, boundary and defects in the periodicity exist. For example, waves generated in the open ocean may impinge on a field of periodic scatterers, or, defects may exist within a large array. Motions of scatterers induced by waves themselves can cause deviations from perfect periodicity, although this effect vanishes at the band gaps where only standing and evanescent modes are excited. Wave structure near edge and defect effects are formally described by imaginary wavevectors for frequencies within the band gaps, *i.e,* there are localized evanescent modes near boundaries and defects. In other words, the full dispersion relation is continued to the complex $\vec{q}-$plane. These boundary and defects lead to localization phenomenon prevalent in many acoustic, electronic, and optical systems.

4. Summary and Conclusions

In this paper, we have presented a simple way of analyzing the dispersion relation for surface flexural-gravity waves in the presence of flexible surface scatterers. The method is adapted from established techniques found in Ashcroft & Mermin (1976), Joanopoulos, Meade & Winn (1995), and Sigalas & Economu (1992) for calculating multiple scattering in electronic, optical, and acoustic phenomena. Figures 2-7 encapsulate the main conclusions of this paper. Our calculations have implicitly included all scattered evanescent modes by solving the problem in discrete Fourier space, and we have treated the most computationally difficult case, that of sharp surface discontinuities. We conclude that: (1). Band gaps can exist in flexural surface scattering of monochromatics waves, (2). The band gaps generally tend to increase with excitation frequency ω, (3). The sensitivity do depth is weak, (4). The sensitivity to f and D_1/D_2 can be strong, where (5). Certain special values of f and D_1/D_2 have vanishing gaps, and (6). The high dispersion in this system prevents the formation of *complete* band gaps in the two-dimensional case. The gaps discussed discussed here are associated with nonpropagating waves and correspond to the "fully resonant" scattering from a finite number of periodic bottom undulations discussed in Davies, Guazzelli & Belzons 1989 where their analyses broke down. Our approach is inherently applicable in the fully reflecting, or resonant regimes (band gaps) although for an infinitely periodic system of *flexible surface* scatterers. Further exploiting the acoustic analogy, we also conclude that complete band gaps do not appear in periodic bottom, shallow water wave scattering. In Appendix A, we related our results with the calculations of reflection R, and transmission T coefficients

of scattering from a *finite* number of surface flexible obstacles. In particular, the relationship between $|T(\omega)|$ and its phase $\delta(\omega)$ was found at all frequencies outside the band gaps. In Appendix B, we considered the possibility of a uniform flow underlying the periodically modulated ice sheet.

Our description of band gaps, frequencies where water waves cease to propagate, imply possible structures for wave damping applications such as breakwaters. Within a large field of periodically spaced flexible plates, the band gaps determine the standing wave response, and reflects all travelling waves from the large field of plates. If a structure embedded in this field is susceptible to transverse wave forces, then it may be desirable to have large band gaps where modes are standing. However, if the periodic surface field is to function as a wave frequency filter, then band gaps are to be avoided in the region of structural resonant frequencies. The important result (5). above suggests that band gaps are generally not monotonic in f and D_2/D_1 and there are special values of these parameters which are to be targeted or avoided depending on the application. Consideration of whether wave generation (by *e.g,* wind) occurs inside the array should be taken as well. Although it appears that no simple complete gaps exist for periodically bottom or surface scattered waves (due to a large dispersion in the surface scattering case, and due to uniform gravity in the shallow bottom scattering case), by appropriately choosing the two-dimensional surface periodicity relative to mean wind directions, one may nonetheless shunt propagating waves for desired band gap frequencies. The effects of directionality of externally impinging and internally generated waves can be inferred from the dispersion relations plotted in Figures 2 and 7. More complicated structures where the basic unit cell of periodicity contains more that one scatterer can be treated by similar methods as described in this paper and elsewhere (Ashcroft & Mermin (1976) and Joanopoulos, Meade & Winn (1995)).

Applications to wave propagation in Marginal Ice Zones (MIZ) may also be interpreted in terms of multiple scattering (see for example Fox & Squire (1990) and Squire et al. (1995)), with the perfect periodicity treated in this paper as an extreme limiting case. Defects in the perfect periodicity can give rise to evanescent localized modes which may be relevant for "Roll-over" and other anomalous effects seen in measurements of wave energy in the MIZ as discussed by Squire et al. (1995) and Wadhams et al. (1988). Further work may extend the analyses to specific problems involving wave forces on surface ice, ice breaking, and wave channelling. It may be feasible to break ice in certain patterns to channel surface water wave energy much like optical waveguides (Joanopoulos, Meade & Winn (1995)).

The author thanks TJ Pedley for bringing to his attention the work of DV Evans, MC Payne for helpful discussions, MG Worster for comments on the manuscript, and Dirk Laurie for checking the numerical code. The author also acknowledges the Wellcome Trust for their support.

Appendix A. Reflection and Transmission in 1D

In the one dimensional periodic scattering problem, the existence of band gaps can be explicitly calculated from considering the reflection R, and transmission T coefficients from a *finite* number n of scatterers. The calculation of R and T in general water wave scattering systems is mathematically difficult, however, in all cases, two of the four unknowns are eliminated via conservation of energy and wave momentum. Here, we derive a relationship between the scattering coefficients and phases of scattering from a *finite* number of scatterers to the exact periodic solutions computed above, and show that in

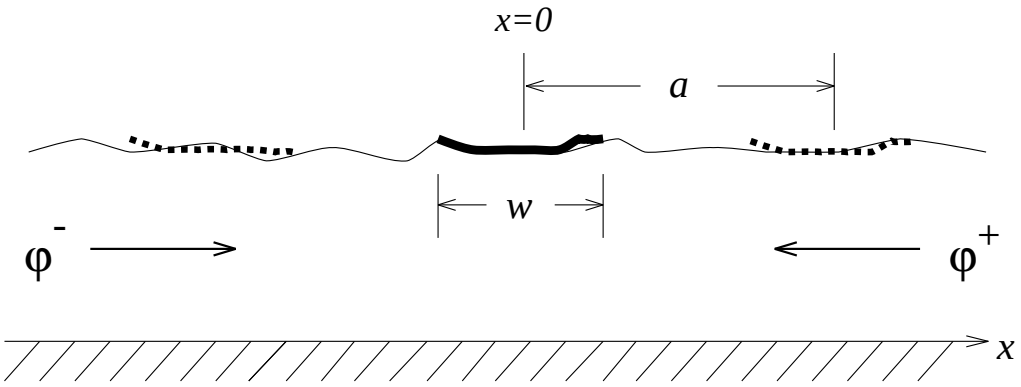

FIGURE 8. Normal incidence scattering from a single ($n = 1$) surface scatterer. The relationship Eqn. (A 9) is valid for any general symmetric one-dimensional scattering problem.

certain reasonable limits, a third condition arises which allows efficient calculation of the reflection and transmission amplitudes and their phases, given any one of them. Therefore, this relationship may be useful when combined with variational calculations of the reflection and transmission amplitudes. This third constraint may also be useful experimentally, when only one of the four unknowns (for single one-dimensional scattering) can be readily measured.

A single scatterer of *general* shape $D(x)$ is depicted in Figure 8 with the only provisions that $D(|x| > w/2) = D_1$ is constant and $D(x) = D(-x)$. Consider n replicas of such surface scatterers centered about $x = 0$. Note that the most general solution to Laplace's equation for $|x| > (n-1)a/2 + w/2$ can be written as a complete set of eigenfunctions

$$\varphi(x, z, \omega) = A_{\pm} e^{\pm i k_0 x} \cosh\, k_0(h+z) + \sum_{n=0}^{\infty} B_n^{\pm} e^{\pm \kappa_n x} \cos\, \kappa_n (h+z) \qquad \text{(A 1)}$$

where k_0 is the positive real root of

$$\left(\frac{D_1}{\rho} k_0^5 + g k_0\right) \tanh k_0 h = \omega^2 \qquad \text{(A 2)}$$

and the κ_n are defined by

$$\left(\frac{D_1}{\rho} \kappa_n^5 - g \kappa_n\right) \tan(\kappa_n h) = \omega^2. \qquad \text{(A 3)}$$

Thus, the far field ($|x| \to \infty$) asymptotic solution consists of travelling (again, the $e^{-i\omega t}$ factor has been suppressed) propagating waves, with the coefficients $A_{\pm}$ related to R and T. In a single scattering problem, we are not interested in the complicated details of the evanescent components $B_n^{\pm}$, except for the fact that they modify the potential and match φ near the scattering region $|x| \sim (n-1)a/2 + w/2$. Since nonpropagating modes decay exponentially according to Eq. (A 3), the longest-ranged mode decays exponentially with a length scale comparable to the depth h. For infinite depth fluids, the infinite number of poles in the complex k plane collapse into a branch cut with the result that the nonpropagating mode now decays $\sim (k_0|x|)^{-6}$. We assume that the wavelength $2\pi/k_0$ or h is small compared to $a - w$ which can be achieved by waves excited at high frequencies

and/or considering small f. The velocity potential in a periodically repeated structure, in the region $|x| \leq na/2$ can be thus written as combinations of single scattering problems with incident waves from $x < -na/2$ and $x > +na/2$, where

$$\begin{aligned}\varphi^- &= e^{ik_0x}\frac{\cosh k_0(h+z)}{\cosh k_0h} + Re^{-ik_0x}\frac{\cosh k_0(h+z)}{\cosh k_0h} + \xi_1(x,z) \qquad x \leq -(n-1/2)a - w/2 \\ &= Te^{ik_0x}\frac{\cosh k_0(h+z)}{\cosh k_0h} + \xi_2(-x,z) \qquad x \geq (n-1/2)a + w/2\end{aligned} \tag{A 4}$$

and

$$\begin{aligned}\varphi^+ &= e^{-ik_0x}\frac{\cosh k_0(h+z)}{\cosh k_0h} + Re^{ik_0x}\frac{\cosh k_0(h+z)}{\cosh k_0h} + \xi_1(-x,z) \qquad x \geq (n-1/2)a + w/2 \\ &= Te^{-ik_0x}\frac{\cosh k_0(h+z)}{\cosh k_0h} + \xi_2(x,z) \qquad x \leq -(n-1/2)a - w/2\end{aligned} \tag{A 5}$$

where the functions ξ_1 and ξ_2 denote the evanescent contributions which in general depend on R and T, decay away from the scatterer, and are small at $x = \pm na/2$. The entire potential in the periodic system is thus

$$\varphi(x,z) = C_1\varphi^- + C_2\varphi^+. \tag{A 6}$$

We apply Bloch's theorem to the potential and v_x for all z across n scatterers and obtain

$$\begin{aligned}\varphi(-na/2) &= e^{inq_xa}\varphi(na/2) \\ \partial_x\varphi(-na/2) &= e^{inq_xa}\partial_x\varphi(na/2).\end{aligned} \tag{A 7}$$

The $\xi_{1,2}$ are chosen such that (A 7) determine C_1 and C_2 for all z. Considering a region straddling the n scatterers far away from the nonpropagating modes; conservation of energy and momentum across its surface ($x \sim \pm na/2$) requires

$$\begin{aligned}|R|^2 + |T|^2 = 1, \\ 1 - R = T\end{aligned} \tag{A 8}$$

respectively. Defining the complex values as $R = |R|e^{i\chi}$ and $T = |T|e^{i\delta}$, (A 8) immediately give $\chi = \delta \pm \pi/2$. Upon substitution of (A 6) into (A 7) and using (A 8), χ, and δ to reduce the result,

$$\frac{\cos(nk_0a + \delta)}{|T|} = \cos nq_xa + O(\xi_{1,2}(na/2)) + O(\xi_{1,2}^2). \tag{A 9}$$

Equation (A 9) represents a condition between $|T|$ and δ when $k_0(\omega)$ and q_x are given. One can readily obtain k_0 from (A 2) and q_x from the results in Section 3. However, only higher bands (higher frequencies) should be used, as these are associated with sufficiently high wavevectors to allow neglect of the evanescent $\xi_{1,2}$ terms away from the scattering edge. Consider the reduced frequency $\omega \simeq 5.45$, and the reduced $q_x = \pi$ (in the repeated zone scheme) of the fifth band (therefore wavelengths $\lambda \leq a/5$) in Fig. 2. We have

$$\cos\left(nk_0(5.45)+\delta(5.45)\right)\simeq(-1)^n|T(5.45)|, \tag{A 10}$$

where k_0 is to be found from (A 2). In general, for any fixed q_x, there are an infinite set (neglecting the lower bands) eigenfrequencies ω such the the functional relationship between $|T(\omega)|$ and $\delta(\omega)$ are identical. The relation (A 9) holds for longer wavelengths if $h \ll a$ since the evanescent modes are shorter ranged.

Appendix B. Uniform Flow

The analyses given in this paper can be easily generalized to cases with uniform current underneath the surface scatterers. The related bottom scattering problem has been studied by Kirby, 1986. The linearized interfacial normal stress due to the fluid in this case is

$$P_{nn}\equiv\rho\left(\partial_t\varphi+\vec{U}_0\cdot\nabla_\perp\varphi+g\eta\right). \tag{B 1}$$

where $\vec{U}_0$ is the uniform stream velocity just beneath the surface. Further derivation will be simplified by considering only a fully material-covered interface, where the surface deformations follow Lagrangian coordinate and are not convected by $\vec{U}_0$. The kinematic condition in this case is identical to Eqn. (2.4). Thus, for the sake of simplicity, we do not consider open water, but can allow for varying thickness in ice cover for example. Since we are considering an ideal fluid, the shear layer becomes infinitely thin and $\vec{U}_0$ contributes only to the normal stress. The effects when there is open water can be easily included by considering $\vec{U}_0(\vec{G})$ as nonzero constant in the open water regions, and zero underneath the scatterers in the kinematic boundary condition *only*. For a fully plate-covered interface ($\sigma=0$), the additional term $\vec{U}_0$ in the $\hat{z}$ component stress balance leads to the generalized eigenvalue equation

$$\det\left|\mathbf{A}-\left(\omega^2-\Omega^2_{\vec{q}}(\vec{G})-\omega\vec{U}_0\cdot(\vec{q}-\vec{G})\right)\mathbf{1}\right|=0, \tag{B 2}$$

which upon defining $\omega\varphi_{\vec{q}}(\vec{G})\equiv\psi_{\vec{q}}(\vec{G})$ can be rewritten in terms of a standard eigenvalue problem for $(\varphi_{\vec{q}}(\vec{G}),\psi_{\vec{q}}(\vec{G}))$ as described in Press (1992). Clearly, only the component of $\vec{q}-\vec{G}$ perpendicular to $\vec{U}_0$ will have inversion symmetry. The band structure will now be more complicated, and the band gaps will in general be different depending on the wavevector direction relative to $\vec{U}_0$.

REFERENCES

Andelman, D. Brochard, F., and Joanny, J-F. 1987 Phase transitions in Langmuir monolayers of polar molecules, *J. Chem. Phys.*, **86**, 3673-3681.

Ashcroft, N. W, and Mermin, N. D. 1976 *Solid State Physics*, (W. B. Saunders, Philadelphia).

Belzons, M., Guazzelli, E., and and Parodi, O. 1988 Gravity waves on a rough bottom:experimental evidence of one-dimensional localization, *J. Fluid Mech.*, **186**, 539-558.

Black, J.L., Mei, C. C., and Bray, M. C. G., 1971 Radiation and scattering of water waves by rigid bodies, *J. Fluid. Mech.,* **46**(1), 151-164.

Chou, T., and Nelson, D. R., 1994 Surface Wave Scattering at Nonuniform Interfaces, *J. Chem. Phys.,* **101**(10), 9022-9032.

Chou, T., Lucas, S. K., and Stone, H. A. 1995. Capillary Wave Scattering from a Surfactant Domain, *Phys. Fluids,* **7**(8), 1872-1885.

Davies, A. G., Guazzelli, E., and Belzons, M. 1989. The propagation of long waves over an undulating bed, *Phys. Fluids A*, **1**(8), 1331-1340.

Devillard, P., Dunlop, F., and and Souillard, B. 1988 Localization of gravity waves on a channel with a random bottom, *J. Fluid Mech.*, **186**, 521-538.

Elter, J. F. and Molyneaux, J. E., 1972 The long-distance propagation of shallow water waves over an ocean of random depth, *J. Fluid. Mech.,* **53**(1), 1-15.

Fernyhough, M. and Evans, D. V. 1995 Scattering by a periodic array of rectangular blocks, *J. Fluid. Mech.* **305**, 263-279.

Fox, C., and Squire, V. A., 1990 Reflection and Transmission Characteristics at the Edge of Shore fast Ice, *J. Geophys. Res.,* **95**(C7), 11629-11,639.

Friedrichs, K. O. and Lewy, H. 1948. The dock problem, *Comm. on Appl. Math.*, **1**, 135-148.

Gou, S., Messiter, A. F., and Schultz, W. W. 1993. Capillary-gravity waves in a surface tensoin gradient. I: Discontinuous change. *Phys. Fluids A* **5**(4), 966-972.

Greene, T. R., and Heins, A. E. 1953 Water waves over a channel of infinite depth, *Q. Appl. Math*, **21**(2), 201-214.

Heins, A. E., 1956 The scope and liitations of the method of Wiener and Hopf, *Comm. Pure and Appl. Math.,* **9**, 447-466.

Hui, P. M. and Johnson, N. F. 1995 Photonic Band-Gap Materials, *Solid State Physics,* **49**, 151-203.

Joannopoulos, J. D., Meade, R. D., and Winn, J., *Photonic Crystals: Molding the flow of Light*, (Princeton Unioversity Press, NJ 1995).

Kagemoto, H., and Yue, D., 1986 Interactions among multiple three-dimensional bodies in water waves: an exact algebraic method, *J. Fluid Mech.*, **166**, 189-209.

Kirby, J. T. 1986 Current effects on resonant reflection of the surface water waves by sand bars. *J. Fluid. Mech.* **186**, 501-520.

Kleinert, P. 1990 A Field-Theoretic treatment of Third-Sound localization, *Phys. Stat. Sol. B,* **168**, 539-550.

Knobler, C. M and Desai, R. C. 1992 Phase transitions in monolayers, *Ann. Rev. Phys. Chem.,* **43**, 207-236.

Krein, M. G. 1962 Integral equations on a half-line with kernel depending upon the difference of the arguments *Translations of the American Math. Society*, **22** 163.

Kushwaha, M. S., Halveli, P., Dobrzynski, L., and Djafari-Rouhani, B. 1993 Acoustic Band Structure of Periodic Composites, *Phys. Rev. Lett.,* **71**(13), 2022-2025.

Liu, A. K. and Mollo-Christensen, E. 1988. Wave Propagation in a Solid Ice Pack, *J. Phys. Oceanogr.*, **18**, 1702-1712.

Lucassen-Reynders, E. H., and Lucassen, J. 1969. *Adv. Coll. Interface Sci.,***126**, 154.

McCall, S. L., Platzmann, P. M., Dalichaouch, R., Smith, D., and Schultz, S. 1991 Microwave Propagation in Two-Dimensional Dielectric Lattices, *Phys. Rev. Lett.,* **67**(15), 2017-2020.

Mei, C. C., Hara, T., and Naciri, M. 1988 Note on the Bragg scattering of water waves by parallel bars on the seabed, *J. Fluid. Mech.,* **16**, 147-162.

Mei, C. C. 1983 *The Applied Dynamics of Surface Ocean Waves* (Wiley, New York).

Mei, C. C. 1985 Resonant reflection of surface water waves by periodic sandbars. *J. Fluid Mech.,* **152**, 315-335.

Meylan, M., and and Squire, V. A. 1994 The response of ice floes to ocean waves, *J. Geophys. Res.*, **99**(C1), 891-900.

Meylan, M. H., and Squire, V. A. 1996. Response of a circular ice floe to ocean waves, *J. Geophys. Res.,* **101**(C4), 8869-8884.

Mitra. A., and and Greenberg, M. D. 1984 Slow interactions of gravity waves and a corrugated sea bed, *J. Appl. Mech.* **51**(2), 251-255.

Naciri, M., and Mei, C. C., 1988 Bragg scattering of water waves by a doubly periodic seabed. *J. Fluid. Mech.,* **192**, 51-74.

Noble, B. 1958 *Methods based on the Weiner-Hopf technique for the solution of partial differential equations,* (Pergamon Press, New York)

Porter, R. and Evans, D. V. 1995 Wave scattering by periodic arrays of breakwaters. *Wave Motion* **23**, 95-120.

Press, W. H., Teukolsky, S. A., Vetterling, W. T., and Flannery, B. P., 1992. *Numerical Recipes*, (Cambridge, England).

Sigalas, M. M. and Economou, E. N. 1992. "Elastic and Acoustic Wave Band Structure," *J.*

Sound and Vibr., **158**(2), 377-382.

Squire, V. A., Dugan, J. P., Wadhams, P., Rottier, P. J., and Liu, A. K. 1995. Of Ocean Waves and Sea Ice, *Ann. Rev. Fluid Mech.,* **27**, 115-168.

Ursell, F. 1957. The transmission of surface waves under surface obstacles. *Proc. Camb. Phil. Soc.,* **57**, 638-668.

Wadhams, P., Squire, V. A., Ewing, J. A., and Pascal, R. W., 1986 The effect of the marginal ice zone on the directional wave spectrum of the ocean, *J. Phys. Oceanogr.,* **16**, 358-376.

Wadhams, P., Squire, V. A., Goodman, D. J., Cowan, A. M., and Moore, S. C. 1988 The attenuation rates of Ocean waves in the Marginal Ice Zone, *J. Geophys. Res.,* **93**(C6), 6799-6818.

Yablonovitch, E., Gmitter, T. J., and Leung, K. M. 1991 *Phys. Rev. Lett.,* **67**, 2295.

Yablonovitch, E. 1994 Photonic crystals, *J. of Mod. Optics*, **41**(2), 173-194.